Materials Science & Engineering A 585 (2013) 292–296

Contents lists available at ScienceDirect

Materials Science & Engineering A

journal homepage: www.elsevier.com/locate/msea

Twin intersection mechanisms in nanocrystalline fcc metals

F. Wu [a], H.M. Wen [b], E.J. Lavernia [b], J. Narayan [a,*], Y.T. Zhu [a]

[a] Department of Materials Science and Engineering, North Carolina State University, Raleigh, NC 27695-7907, USA
[b] Department of Chemical Engineering and Materials Science, University of California, Davis, CA 95616, USA

ARTICLE INFO

Article history:
Received 18 June 2013
Received in revised form
18 July 2013
Accepted 22 July 2013
Available online 31 July 2013

Keywords:
Nanocrystalline materials
Twin intersection
HRTEM
Dislocation reaction

ABSTRACT

Deformation twins have been reported to produce high strength and ductility. Intersections of deformation twins may affect the microstructural evolution during plastic deformation and consequently influence mechanical properties. However, the mechanisms governing twin-intersection behavior remain poorly understood. In this study, we investigated twin intersection mechanisms by observing twin transmission across the boundary of another twin using high-resolution transmission electron microscopy. Based on the experimental observations, mechanisms were proposed for twin–twin intersections and associated dislocation reactions in nanocrystalline fcc materials.

© 2013 Elsevier B.V. All rights reserved.

1. Introduction

When one twin meets another twin, what mechanism governs their intersection? This problem is interesting because deformation twinning in nanocrystalline (NC) materials is of both fundamental and technological significance. Experimental observations [1–4] and molecular dynamics (MD) simulations [5,6] reveal that deformation twins will interact with gliding dislocations, which simultaneously increases the strength and ductility of NC materials [2,7]. In NC face-centered cubic (fcc) metals, deformation twinning has been observed under various deformation conditions, including low temperature [8], high strain rate [9], high-pressure torsion [10–12], uniaxial tensile testing [13] and cryogenic ball milling [14]. Moreover, it has been reported that for NC fcc metals, twinning becomes a major deformation mechanism within a range of grain sizes [15–19].

When multiple twinning systems are activated in fcc metals, interactions between various twinning systems become inevitable. This not only affects the microstructural evolution but also is expected to affect the mechanical behavior of the material during deformation. Twin intersections have been observed in fcc stainless steel [20] and Hadfield steel single crystals [21]. These experimental observations raise a critical question: what is the dislocation mechanism associated with the observed twin intersections?

To answer the above question, we studied intersections of twins in NC Cu film and Cu–30 wt% Zn–0.8 wt% Al alloy (Brass 260, Cartridge Brass) samples using high-resolution transmission electron microscopy (HRTEM). These two material systems were selected because NC Cu has been reported to easily form deformation twins [22–24], and the Brass 260 alloy has lower stacking fault energy than Cu and also easily forms deformation twins and twin intersections [25]. To study the intersection mechanism of twins, we have obtained clear HREM images at locations where one twin transmits across the coherent boundary of another twin. This requires a low dislocation density around the observed region to reduce lattice distortions. Detailed sample preparation procedures to meet this requirement are described in the next section.

2. Experimental procedure

Both an NC Cu film and NC Brass 260 alloy samples were used in this study. The NC Cu film was deposited on a coarse-grained Cu substrate using pulsed laser deposition (PLD). The coarse-grained Cu substrate was used so that it deformed evenly with the NC Cu film under uniaxial tension to a designated strain. The PLD processing parameters can be found in a previous paper [26]. The NC Cu film was strained under tension together with the substrate at a strain rate of $2.5 \times 10^{-4}\ s^{-1}$ to a plastic strain of 1.5%. Such a small tensile strain was chosen to reduce the density of accumulated dislocations at twin boundaries so that clear HREM images can be obtained from the area of twin intersections.

The NC Brass 260 alloy was processed by cryo-milling and spark plasma sintering (SPS). The SPS serves two purposes: to consolidate the alloy powder for easier HRTEM sample preparation and to reduce dislocation density for higher quality HRTEM images. Dislocations formed during cryo-milling are mostly annihilated during

* Corresponding author. Tel.: +1 919 513 0559.
E-mail address: narayan@ncsu.edu (J. Narayan).

0921-5093/$ - see front matter © 2013 Elsevier B.V. All rights reserved.
http://dx.doi.org/10.1016/j.msea.2013.07.063

the high-temperature SPS process so that the deformation twin boundaries become more coherent and straight [25]. The detailed processing parameters can be found in a previous publication [25].

Special care was taken during the sample preparation so that no extra dislocations were introduced into the final TEM sample. TEM specimens were prepared by mechanical grinding and dimpling, followed by ion milling. Low-energy ion beam was used for ion milling to minimize the irradiation damage by the ion beam and to remove the deformed surface layer on the TEM sample. HRTEM investigations were performed on JEOL analytical electron microscopes operating at 200 kV, with point to point resolution of 0.18 nm. Details on HRTEM sample preparation can be found in our previous publications [25,26].

3. Results and discussion

3.1. TEM and HRTEM observation of twin transmission across twin boundary

Fig. 1(a) is a typical HRTEM image showing a twin transmitting across the boundary of another twin in the NC Cu film that was fabricated by PLD and subsequently deformed to plastic strain of 1.5% by uniaxial tension. Fig. 1(b) is an HRTEM image enlarged from the twin transmission area in Fig. 1(a) and is marked for the convenience of description. The ITB and TTB stand for the incident twin boundary and transmittal twin boundary, respectively. BTB and MTB represent the barrier twin boundary and the migrated twin boundary of the barrier twin, respectively. ω is the angle between the TTB and MTB, and θ is the angle between the BTB and MTB. The d_{IT} and d_{TT} are the twin thicknesses of incident twin (IT) and transmittal twin (TT), respectively. Suppose the upper section of BTB is the original BTB before twin transmission and IT is the twin to whose side that BTB migrates. As shown in Fig. 1(b), the IT penetrates the BTB from the right side of BTB and after reactions with the BTB, it transforms into a TT on the left-hand side of the BTB. The twinning planes for IT and TT are different {111} planes so that the ITB forms an angle of $\sim 141^\circ$ with the TTB. The BTB, ITB and TTB are coherent twin boundaries on {111} slip planes, while MTB deviate from the original BTB. As shown in Fig. 1(b), the reaction between IT and BTB caused the migration of the BTB towards the IT side to form MTB when IT transmitted across the BTB. The MTB in Fig. 1(b) is a straight line lying between the IT and TT, and is also the bisector of the angle between BTB and TTB, which in this case means $\omega=\theta=35.25^\circ$. d_{IT} and d_{TT} were measured from the HRTEM micrograph as 6.3 ± 0.5 nm and 3.6 ± 0.5 nm, respectively, which leads to a ratio of $d_{IT}/d_{TT} \cong 1.7$.

Fig. 1(c) is a typical TEM image showing twin transmission in Brass 260 alloy processed by cryo-milling and spark plasma sintering. An incident twin (IT) first penetrates the BTB from the top left corner of the image and after reacting with the BTB, transforms into a TT along another {111} plane. The TT then meets and reacts with another BTB, but does not transmit across the second BTB. Fig. 1(d) is an HRTEM image enlarged from the MTB area in Fig. 1(c). Unlike the situation shown in Fig. 1(b), the MTB here can be divided into two sections. In the upper section (marked as MTB1), no migration of BTB occurred and therefore MTB1 coincide with the BTB. Both d_{TT1} and d_{IT1} were measured from the HRTEM micrograph to be 3.8 ± 0.3 nm, which indicates that the thickness of the IT is maintained as it transmitted across the BTB to form TT. In the second section, the MTB2 deviates from the BTB by an angle of $\theta \approx 43^\circ$. We measured d_{IT2} and d_{TT2} from

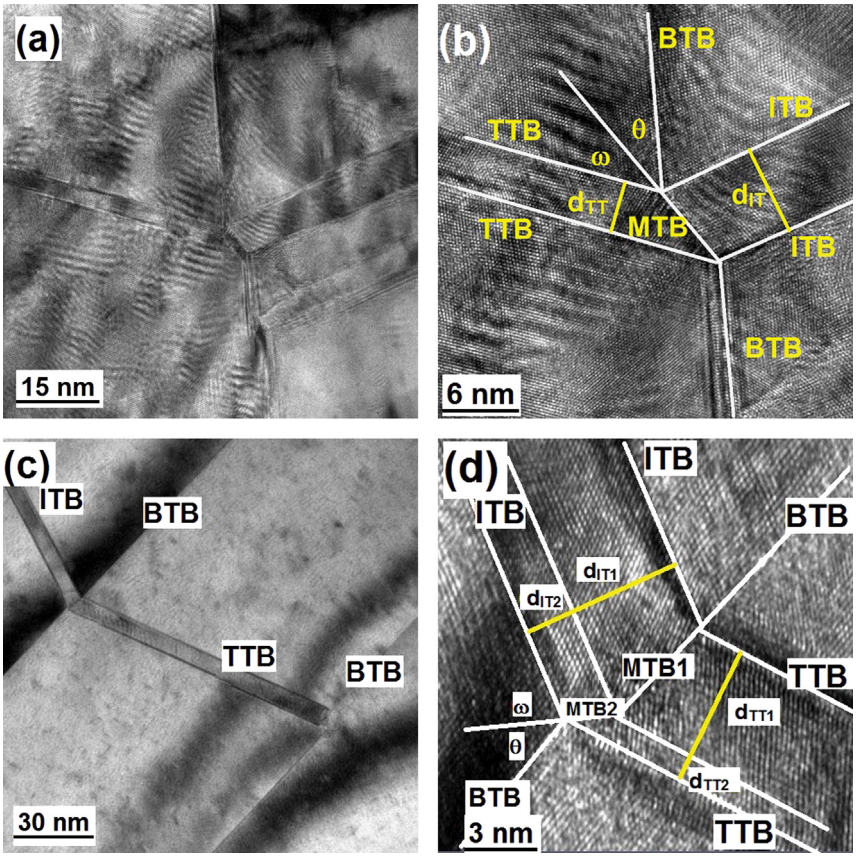

Fig. 1. (a) A typical HRTEM image showing twin transmission phenomenon in NC Cu films processed by PLD and the subsequent uniaxial elongation; (b) the HRTEM image showing the transmission area shown in (a) with marks added; (c) a typical TEM image showing twin transmission phenomenon in NC Brass 260 alloy processed by cryo-milling and the following SPS; (d) the HRTEM image showing the twin transmission area in (c) with marks added.

Fig. 1(d) as 1.7±0.2 nm and 0.8±0.1 nm, respectively, which leads to a ratio of $d_{IT2}/d_{TT2} \cong 2$.

3.2. Possible dislocation reactions at the intersection of two twin boundaries

To better understand the twin transmission mechanism, we need to refer to the double Thompson tetrahedron [27,28], which is shown in Fig. 2. The ITB, BTB and TTB planes correspond to BCD, ABC and BCD′ planes in Fig. 2, respectively. α, β, γ and δ stand for centroids of triangles in the Thompson tetrahedron. For the formation of ITB, Shockley partials need to be emitted from grain boundaries and glide on BCD planes toward the ABC plane under an applied stress. When a Shockley partial reaches the ABC plane, its dislocation line runs parallel to the intersection line of plane BCD and ABC, which is line BC ($<110>$ direction). The Shockley partial can be of the following two types: (1) a 30° Shockley partial dislocation (either **Cα** or **Bα** on BCD plane), or (2) a 90° Shockley partial dislocation (**Dα** on BCD plane). The Shockley partials can either cross-slip onto the ABC plane or transmit onto the BCD′ plane and then glide away from plane ABC to form a TT. Since the twin transmission occurs due to dislocation reactions at the intersection of two twin boundaries, the reactions of twin partial dislocations are actually interactions between dislocations and the twin boundary, which have been analyzed in our previous paper [28]. As described in the paper [28], four types of dislocation reactions are possible to occur:

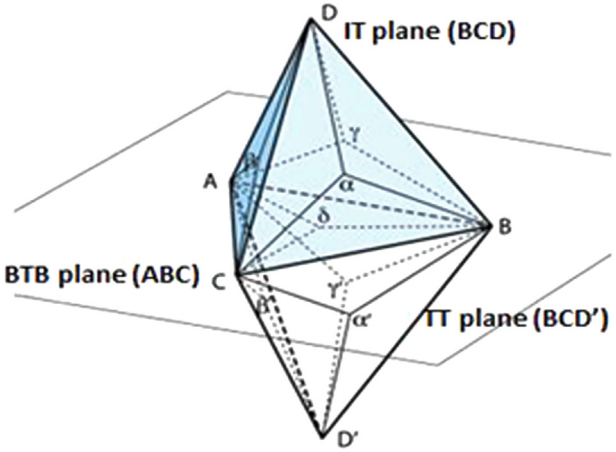

Fig. 2. Schematic illustration of a double Thompson tetrahedron.

$$\mathbf{B\alpha} \rightarrow \mathbf{B\alpha'} + \boldsymbol{\alpha'\alpha} \quad (1)$$

$$\mathbf{B\alpha} \rightarrow \mathbf{B\delta} + \boldsymbol{\delta\alpha} \quad (2)$$

$$\mathbf{D\alpha} \rightarrow \boldsymbol{\alpha'}\mathbf{D'} + 4/9\mathbf{A\delta} \quad (3)$$

$$\mathbf{D\alpha} \rightarrow \mathbf{A\delta} \quad (4)$$

Eqs. (1) and (2) describes the transmission and cross-slip mechanisms of a 30° Shockley partial dislocation gliding on the BCD plane. Both of them generate a sessile stair-rod dislocation, which will stay on the ABC plane. Eqs. (3) and (4) describe the transmission and cross-slip mechanisms of a 90° Shockley partial dislocation gliding on the BCD plane. When a Shockley partial dislocation on the BCD plane cross-slips onto the ABC plane, its sequential movement will move BTB by one atomic plane. The energy barriers for these dislocation–twin reactions have been discussed in the previous publication [28].

3.3. Explanation of the experimentally observed twin transmissions

The experimentally observed twin transmission phenomena can be understood with the help of HRTEM images and the above analysis. From Fig. 1(b), we found that the IT is 30 atomic planes thick, while the TT is only 17 atomic planes thick. This means that a total of 30 partials glided on different BCD planes to form the IT, but only 17 of them transmitted across the BTB. Suppose M and N are the numbers of planes inside IT and TT, respectively, the ratio of M to N is $\cong 1.76$. It is worth noting that planes in IT and TT are all {111} planes so that the ratio between d_{IT} and d_{TT} are equal to the ratio of M to N. The MTB in Fig. 1(b) bisects the angle between BTB and TTB, so that $\theta = 35.25°$. This configuration is schematically illustrated in Fig. 3(a), in which $M=9$ and $N=5$ lead to a ratio of 1.8 between M and N, which is close to the experimentally obtained ratio. Various combinations of dislocation reactions may lead to this configuration. However, a combination of five dislocation reactions according to Eq. (3) and four reactions according to Eq. (4) produces an MTB with the lowest energy,

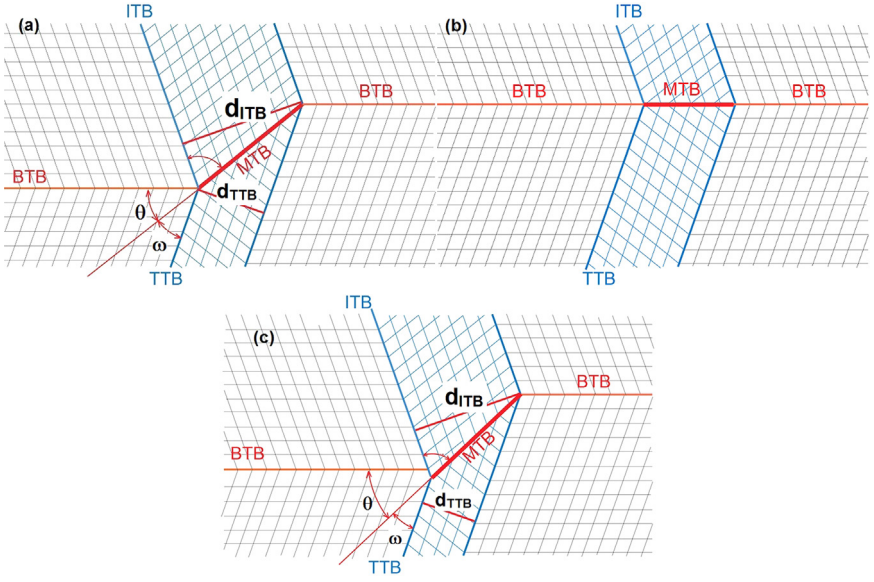

Fig. 3. Schematic illustrations of twin transmission phenomena with (a) $\theta = 35.25°$, (b) $\theta = 0°$, and (c) $\theta = 43°$.

i.e. the lowest residual dislocation content on the MTB:

$$9\mathbf{D\alpha} \rightarrow 5\mathbf{\alpha' D'} + 6\mathbf{A\delta} + 2/9\mathbf{A\delta} \quad (5)$$

Eq. (5) generates six 90° Shockley partial dislocations on plane ABC so that the gliding of them will move BTB by six atomic planes, which is consistent with the schematic illustration in Fig. 3(a). The residual dislocation on MTB is only 2/9**Aδ** for every 9 partials on adjacent BCD planes, which makes this MTB energetically very stable.

The twin transmission phenomenon in Brass 260 alloy processed by cryo-milling and SPS can also be explained with similar analysis of the HRTEM image shown in Fig. 1(d). As discussed earlier, the MTB here has two sections. The MTB1 coincides with the original BTB, for which both the IT and TT have the same thickness of 18 atomic planes. This indicates that a total of 18 partials gliding on BCD planes reached plane ABC, and all of them transmitted across the BTB, which led to an M to N ratio of 1. This scenario is schematically illustrated in Fig. 3(b), in which $M=N=6$. As shown in Fig. 3(b), the ITB, TTB and BTB are all coherent twin boundaries, but the MTB is a semi-coherent twin boundary in nature. Since no steps were generated on BTB, the possible dislocation reaction is described by Eq. (3), and this reaction happens on every slip plane for the twin to transmit across the BTB. This also led to a 4/9**Aδ** residual dislocation on every plane at the MTB1. Therefore, this MTB is a high-energy boundary.

In the second section, the BTB migrates towards the IT side to form MTB2 in Fig. 1(d) with an angle of $\theta \sim 43°$ with the original BTB. From the previous discussion, the ratio of $M/N = d_{IT2}/d_{TT2} = 2/1$. This is schematically illustrated in Fig. 3(c), in which $M=8$, $N=4$. However, MTB is incoherent in this case, which is caused by the high residual dislocation content, as described below. This twin transmission phenomenon can be produced by a combination of equal number of dislocation reactions described by Eq. (2) and by Eq. (3):

$$4\mathbf{B\alpha} + 4\mathbf{D\alpha} = 4\mathbf{B\delta} + 4\mathbf{\delta\alpha} + 4\mathbf{\alpha' D'} + \mathbf{A\delta} + 7/9\mathbf{A\delta} \quad (6)$$

For every eight twinning partials gliding on the BCD planes, four of them are transmitted to the BCD′ planes and 5 partials are generated on plane ABC so that BTB migrates towards the IT side by 5 atomic planes, which is consistent with the illustration in Fig. 3(c). The residual dislocations on MTB are 7/9**Aδ** and 4**δα**. Therefore, compared with the MTB in Fig. 3(a), this MTB has a higher energy.

The proposed dislocation-reaction mechanisms have residual dislocation components on the MTB, which causes lattice distortion (elastic strain) near MTB and consequently reduces the coherency of MTB, as illustrated schematically in Fig. 3. The lattice distortion in the MTB region is clearly visible in the HRTEM images, as shown in Fig. 4, which are enlarged from the MTB areas in Fig. 1. The contrast difference around the MTB regions also shows evidence of elastic strain. Fig. 4a shows the region of the 35° MTB from Fig. 1(b). It can be seen that the MTB is not as sharp or as straight as a coherent twin boundary. Based on fast Fourier transform (FFT) analysis, we found that a total of 3 dislocations exist on MTB. Furthermore, they appear regularly spaced by 9 to 11 {111} planes. This is consistent with the proposed mechanism as described by Eq. (5). Due to the low density of residual dislocations at MTB, i.e., a 2/9**Aδ** residual dislocation for every 9 slip planes according to Eq. (5), the lattice distortion is relatively low. This configuration is stable and has the lowest energy.

Fig. 4(b) shows the enlarged region of MTB in Fig. 1(d), in which MTB first coincides with BTB and then forms an angle of ~43° with BTB. As shown, the atomic image close to the MTB is more blurred than those far away from the MTB, indicating a high lattice distortion caused by high local elastic strain. This is consistent with the high residual dislocation content on the MTB as discussed previously. In addition, both the 43° MTB and 0° MTB appear crooked instead of linear because these two configurations have relatively high energy and are not stable. This is also evident in the schematic illustration in Fig. 3(c), in which lattice cannot match perfectly at MTB.

Generally speaking, if an MTB deviates from the BTB, the twin thickness (d_{IT} and d_{TT}), the number of planes (M and N), and θ will have the following relationship according to the geometric relationship shown in Fig. 3(a):

$$d_{IT}/d_{TT} = M/N = \sin(109.5° - \theta)/\sin(70.5° - \theta) \quad (7)$$

Eq. (7) can be used to analyze twin transmission phenomenon in other twin transmission scenarios observed in the future, allowing the prediction of θ and other variables.

4. Summary

In an fcc system, twin transmission occurs through partial dislocation reactions at the twin boundary. If not all of the partials transmit across the twin boundary, the twin boundary will deviate from the original configuration. The deviation angle is related to the ratio between the number of incident partials and that of transmitted partials. Therefore, the observations and mechanisms reported here can be used to explain twin intersections in fcc metals.

Acknowledgments

JN, YTZ and FW acknowledge the support by the National Science Foundation of the United States (Grant no. DMR41104667). HMW and EJL acknowledge financial support from the Office of Naval Research (N00014-08-1–0405 and N00014-12-1–0237).

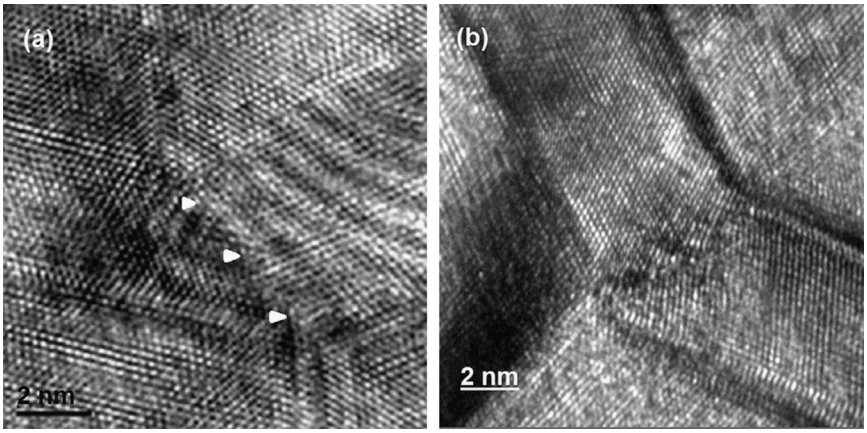

Fig. 4. (a) An HRTEM image enlarged from the MTB area in Fig. 1a; (b) an HRTEM image enlarged from the MTB area in Fig. 1c.

References

[1] K. Lu, L. Lu, S. Suresh, Science 324 (2009) 349–352.
[2] L. Lu, Y.F. Shen, X.H. Chen, L.H. Qian, K. Lu, Science 304 (2004) 422–426.
[3] M. Sennour, S. Lartigue-Korinek, Y. Champion, M.J. Hytch, Philos. Mag. 87 (2007) 1465–1486.
[4] Y.T. Zhu, J. Narayan, J.P. Hirth, S. Mahajan, X.L. Wu, X.Z. Liao, Acta Mater. 57 (2009) 3763–3770.
[5] J. Jin, S.A. Shevlin, Z.X. Guo, Acta Mater. 56 (2008) 4358–4368.
[6] I. Shabib, R.E. Miller, Acta Mater. 57 (2009) 4364–4373.
[7] Y.H. Zhao, Y.T. Zhu, X.Z. Liao, Z. Horita, T.G. Langdon, Appl. Phys. Lett. 89 (2006) 121906.
[8] J.W. Christian, S. Mahajan, Prog. Mater. Sci. 39 (1995) 1–157.
[9] M.A. Meyers, O. Vohringer, V.A. Lubarda, Acta Mater. 49 (2001) 4025–4039.
[10] X.Z. Liao, Y.H. Zhao, Y.T. Zhu, R.Z. Valiev, D.V. Gunderov, J. Appl. Phys. 96 (2004) 636–640.
[11] X.Z. Liao, Y.H. Zhao, S.G. Srinivasan, Y.T. Zhu, R.Z. Valiev, D.V. Gunderov, Appl. Phys. Lett. 84 (2004) 592–594.
[12] Y.T. Zhu, X.Z. Liao, Appl. Phys. Lett. 86 (2005) 103112.
[13] X. Wu, Y.T. Zhu, M.W. Chen, E. Ma, Scr. Mater. 54 (2006) 1685–1690.
[14] X.Z. Liao, F. Zhou, E.J. Lavernia, D.W. He, Y.T. Zhu, Appl. Phys. Lett. 83 (2003) 5062–5064.
[15] Z. Shan, E.A. Stach, J.M. Wiezorek, J.A. Knapp, D.M. Follstaedt, S.X. Mao, Science 305 (2004) 654–657.
[16] S. Hai, E.B. Tadmor, Acta Mater. 51 (2003) 117–131.
[17] R.J. Asaro, S. Suresh, Acta Mater. 53 (2005) 3369–3382.
[18] X. Wu, Y. Zhu, Phys. Rev. Lett. 101 (2008) 025503.
[19] J.-Y. Zhang, G. Liu, R.H. Wang, J. Li, J. Sun, E. Ma, Phys. Rev. B 81 (2010) 172104.
[20] T. Roland, D. Retraint, K. Lu, J. Lu, Mater. Sci. Eng. A-Struct. Mater. Prop. Microstruct. Process. 445 (2007) 281–288.
[21] C. Efstathiou, H. Sehitoglu, Acta Mater. 58 (2010) 1479–1488.
[22] Y.T. Zhu, X.Z. Liao, X.L. Wu, Prog. Mater. Sci. 57 (2012) 1–62.
[23] Y.T. Zhu, X.Z. Liao, S.G. Srinivasan, E.J. Lavernia, J. Appl. Phys. 98 (2005) 034319.
[24] Y.T. Zhu, X.Z. Liao, X.L. Wu, J. Narayan, J. Mater. Sci. 48 (2013) 4467–4475.
[25] H.M. Wen, E.J. Lavernia, Scr. Mater. 67 (2012) 245–248.
[26] F. Wu, Y. Zhu, J. Narayan, http://dx.doi.org/10.1080/14786435.2013.829251, accepted for publication.
[27] Y.B. Wang, B. Wu, M.L. Sui, Appl. Phys. Lett. 93 (2008) 041906.
[28] Y.T. Zhu, X.L. Wu, X.Z. Liao, J. Narayan, L.J. Kecskés, S.N. Mathaudhu, Acta Mater. 59 (2011) 812–821.